CARBON 57 (2013) 395–400

Available at www.sciencedirect.com

SciVerse ScienceDirect

journal homepage: www.elsevier.com/locate/carbon

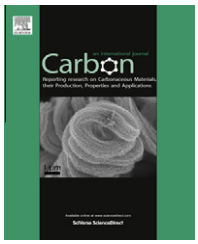

Photoresist-derived porous carbon for on-chip micro-supercapacitors

Ben Hsia, Mun Sek Kim, Maxime Vincent [1], *Carlo Carraro, Roya Maboudian* [*]

Department of Chemical and Biomolecular Engineering, 201 Gilman Hall, University of California, Berkeley, CA 94720, USA

ARTICLE INFO

Article history:
Received 17 September 2012
Accepted 31 January 2013
Available online 9 February 2013

ABSTRACT

Photoresist, which is frequently used in existing microelectronics processing, can be pyrolyzed to form a conductive carbon film. We demonstrate that a pyrolysis technique of SPR-220 photoresist, consisting of heating in Ar ambient to 900 °C followed by further annealing in an H_2/Ar mixture, results in a high surface area porous carbon, applicable to supercapacitor electrode fabrication. Electrochemical testing of the pyrolyzed photoresist film yields a specific areal capacitance of 1.5–3.5 mF/cm^2 and a specific volumetric capacitance of 15–35 F/cm^3. These results are obtained on the as-pyrolyzed films, without additional activation or deposition of electroactive species. The cycling stability of the films is shown to be robust over 10,000 cycles. This photoresist pyrolysis process could be readily integrated into microelectromechanical systems or microelectronics technology for on-chip energy storage.

1. Introduction

Supercapacitors, also known as electrical double-layer capacitors or ultracapacitors, have attracted significant research interest due to their fast cycling and long lifetime relative to current battery technology, charging and discharging in seconds (vs. hours for batteries) for millions of cycles (vs. thousands of cycles for batteries) [1]. With these characteristics, supercapacitors can fill a crucial energy storage niche for applications that require high power density or long lifetime such as energy harvesting from the braking of vehicles or powering sensors in harsh environments where frequent device replacement would be undesirable. Supercapacitors, which rely on charge storage at the electrode–electrolyte interface (rather than in the electrode bulk, as in batteries), can achieve capacitance values between 5 and 20 μF/cm^2 real surface area, which necessitates high specific surface area electrodes to achieve practical energy densities [1]. For this reason, supercapacitor electrodes are commonly composed of highly porous carbon materials due to their high specific surface area and good conductivity [2,3]. However, for powering microsensors or other microdevices, a scalable technique for deposition and patterning of this highly porous carbon material must be developed to enable on-chip integrated micro-supercapacitors. Some proposed carbon-based electrode materials for micro-supercapacitors include ink-jet printed activated carbon, CNTs, graphene, and carbide-derived carbon [4–9]. While these techniques hold promise, each approach presents significant fabrication challenges: ink-jet printing requires complex synthesis and binder materials and may be difficult to scale, carbon nanotubes are difficult to grow controllably and have high contact resistances with most substrates, graphene requires high temperatures or transfer processes to fabricate, and carbide-derived carbon involves a lengthy fabrication with multiple deposition and patterning steps.

In this letter, we describe a simple and scalable method for synthesis of a porous, high surface area carbon material whose properties resemble those of activated carbon and that is easily patternable and amenable to on-chip integration.

[*] *Corresponding author:* Fax: +1 510 642 4778.
E-mail address: maboudia@berkeley.edu (R. Maboudian).
[1] Current address: Tronics Microsystems, 98 rue du Pré de l'Horme, 38926 Crolles, France.
0008-6223/$ - see front matter
http://dx.doi.org/10.1016/j.carbon.2013.01.089

The synthesis procedure utilizes a photoresist pyrolysis technique that is akin to the fabrication of carbon-based MEMS devices [10–12]. Other efforts to use pyrolyzed photoresist as a supercapacitor electrode material have yielded very low specific capacitance values (<0.1 mF/cm^2) prior to electrochemical activation, deposition of an active material, and/or patterning of high aspect ratio 3D microstructures [13–15]. Whereas these previous studies primarily utilize H_2/N_2 forming gas for the pyrolysis environment, we demonstrate that a two-step process using Ar followed by H_2/Ar at 900 °C yields significantly improved capacitive performance.

2. Experimental

The synthesis of the porous carbon layer consists of two primary steps, photoresist deposition and pyrolysis, as shown in Fig. 1. SPR-220-7 photoresist (MicroChem) is spin-coated at 1800 rpm to a thickness of ~10 μm (as determined by profilometry) on a Si substrate. This is followed by a 3 min soft bake at 115 °C on a hot plate. If patterning is desired, the photoresist can then be patterned using standard lithographic techniques before pyrolysis. After photoresist deposition (and optional patterning), the sample is loaded into a hot-wall CVD furnace (Thermo Scientific Lindberg Blue M), prebaked at 300 °C in ~1 Torr Ar (Praxair), for 30 min. This prebake is intended to drive off water and volatile solvents [16–18] in order to reduce the formation of macroscale gas bubbles in the film during pyrolysis. Then, the temperature is increased to 900 °C in the same ambient at an approximate rate of 40 °C/min. Once 900 °C is reached, the gas is changed to 10% H_2/90% Ar (Praxair) and the sample is held at 900 °C for 1 h. This change in gaseous pyrolysis ambient at the pyrolysis temperature contrasts crucially with previous photoresist pyrolysis studies which used only one gas throughout, primarily H_2/N_2 [10,13–15]. The sample is then cooled at a rate of about 25 °C/min to room temperature in the same H_2/Ar gas environment. It should be noted that pyrolysis temperatures of 800 and 1000 °C are also tested, but yield inferior capacitance results, leading to the selection of 900 °C as an optimal temperature.

After pyrolysis, a copper wire is contacted to the surface of the unpatterned film using silver epoxy and the electrochemical properties of the film are studied via a commercial potentiostat (CH Instruments, 660D Model) in 3.5 M KCl solution with an Ag/AgCl reference electrode and Pt wire counter electrode. The film's physical properties are further studied via Raman spectroscopy (HORIBA Jobin Yvon LabRam), 4-point sheet-resistance probe (Signatone S-301-4), atomic force microscopy (Digital Instruments Nanoscope IIIa), and X-ray photoelectron spectroscopy (Omicron). Water contact angle (Rame Hart 100) measurements are used to determine the wettability of the pyrolyzed samples. In order to minimize the effect of surface contamination, samples are sonicated in isopropyl alcohol followed by sonication in deionized water and thorough N_2 drying immediately before contact angle measurements.

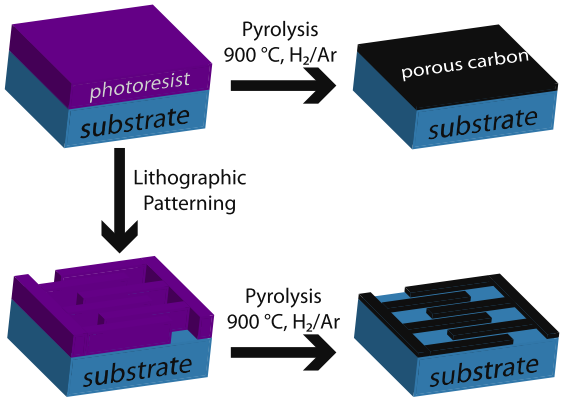

Fig. 1 – Process schematic for synthesis of unpatterned and patterned porous carbon electrodes.

3. Results

Fig. 2 shows an optical image of patterned photoresist on a Si substrate before and after annealing and a cross-sectional scanning electron micrograph (SEM) of the annealed photoresist.

While the thickness decreases from ~10 to ~1 μm during pyrolysis (measured via cross-sectional SEM), the footprint of the electrode remains approximately the same due to good adhesion with the underlying substrate, highlighting that standard photolithography techniques can be employed effectively. Raman spectroscopy confirms the carbonaceous nature of the pyrolyzed material (as seen in Fig. 3) with signature graphitic D- and G-peaks around 1350 and 1600 cm^{-1}, respectively. A characteristic Raman spectrum of commercial activated carbon (Sigma Aldrich) is shown for comparison. Atomic force microscopy (AFM) analysis shows a smooth film surface which has a root-mean-square roughness of 0.5 nm over a scan range of 2 × 2 μm^2. This relatively smooth surface morphology is similar to that observed for previous photoresist pyrolysis studies [13]. Four-point probe yields a sheet resistance of 120 Ω/□ for 1-μm thick pyrolyzed material.

Cyclic voltammetry (CV) experiments show good capacitive behavior at all measured scan rates. A representative

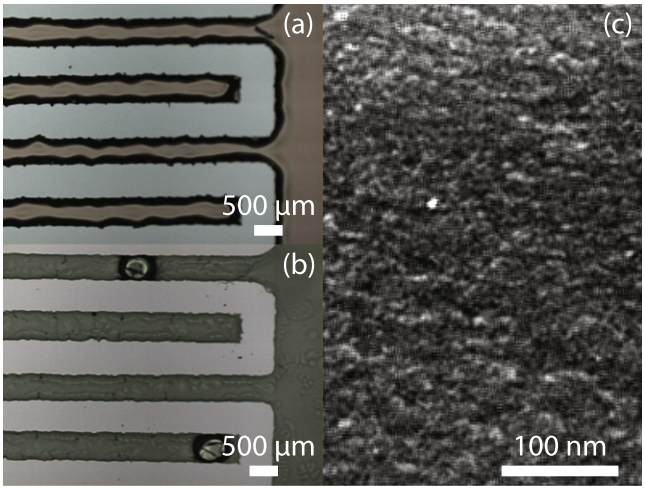

Fig. 2 – Optical image of patterned SPR-220 photoresist (a) before and (b) after pyrolysis. (c) Cross-sectional SEM image of pyrolyzed photoresist.

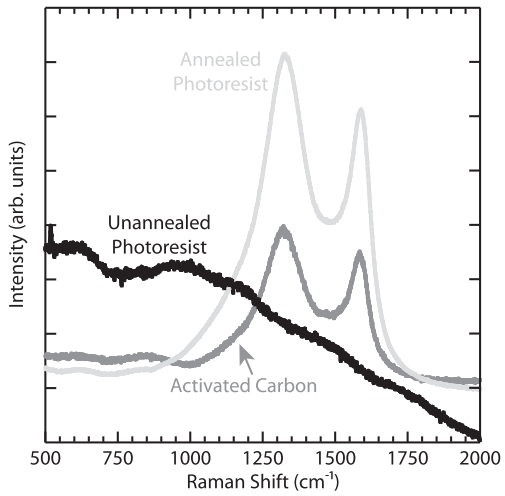

Fig. 3 – Raman spectra of photoresist, pyrolyzed photoresist, and commercial activated carbon for comparison. Pyrolyzed photoresist and activated carbon share similar peak shape and location, with broad D- and G-peaks at 1350 and 1600 cm^{-1}, respectively.

behavior is shown in Fig. 4a for three scan rates in 3.5 M KCl aqueous electrolyte. The sharp peaks at the extreme edges of the voltage window likely result from the oxidation/reduction processes of the aqueous electrolyte and do not contribute to pseudocapacitive energy storage. However, the reversible reduction and oxidation of oxygen containing moieties at the carbon surface is probably responsible for the current increases observed around −0.1 V and +0.6 V and has been previously reported in other carbon based electrodes [14,19]. These functional groups are likely generated during pyrolysis due to the high oxygen content of phenolic photoresists and contribute to pseudocapacitance. The disappearance of these peaks at high scan rates indicates that these faradaic processes are likely kinetically limited. The rounding-off of the CV curve at the initiation of the cathodic and anodic sweeps for the 1 V/s scan is a result of equivalent series resistance (ESR), which will be discussed later in further detail. Specific capacitance values are calculated from the CV scans by Eq. (1):

$$C = \frac{I}{dV/dt}\frac{1}{A} \quad (1)$$

where C is the specific capacitance in F/cm^2, I is the current magnitude averaged over the positive and negative sweep range in A, dV/dt is the bias sweep rate in V/s, and A is the electrode projected area in cm^2. The measured specific capacitance of a 1 μm film is determined to be between 1.5 and 3.5 mF/cm^2 for all measured scan rates, resulting in a volumetric capacitance in the range of 15–35 F/cm^3 (see Fig. 4b). The decrease in capacitance at high scan rates can be attributed to a combination of factors including the kinetically limited pseudocapacitive reactions mentioned earlier and diffusion limited charge transport in the film's micropores [20].

As a further probe of the electrochemical properties of the film, galvanostatic charge discharge cycles are performed (Fig. 4c). The electrode is charged and discharged at a constant current, and the voltage is measured. The capacitance can also be calculated from these measurements using Eq. (1); in the case of galvanostatic discharge, dV/dt is approximated by ΔV/Δt (as shown in the figure), the inverse of the amount of time required to fully discharge the film at constant current [21]. For currents of 0.5, 1, and 5 mA/cm^2, the specific capacitance is calculated to be 3.2, 3.0, and 2.1 mF/cm^2, respectively, in good agreement with the capacitance values obtained from the CV measurements. The non-linearity of the charge and discharge curves confirms the contribution of pseudocapacitive faradaic reactions to the capacitance, as an ideally polarizable electrode with no charge transfer to the electrolyte would have linear charge and discharge curves. The galvanostatic measurements additionally provide quantitative information about the ESR. The rapid change in current at the start of each charge/discharge half cycle is commonly termed the IR drop and is indicative of an ohmic resistance, which can be attributed to electrode resistance, contact resistance, and electrolyte resistance. ESR can be estimated from the IR drop by dividing the voltage drop by twice the current [21], resulting in the value of about 40 Ω for a 0.32 cm^2 sample with 1-μm thick pyrolyzed material. AC impedance spectroscopy (ACI, Fig. 4d) can also be used to estimate ESR, by measuring the impedance at frequencies approaching ∞ [22]; due to the limitations with our potentiostat, the high frequency limit beyond 1 MHz is not accessible, but by extrapolating the apparent Nyquist semi-circle to the high frequency limit, an ESR value of about 25 Ω is obtained, which is in reasonable agreement with the estimates from galvanostatic charge/discharge measurements. ESR limits a device's maximum power, and the high ESR measured here likely results from diffusional resistance in pores [20] as well as the relatively high sheet resistance of the pyrolyzed photoresist film (120 Ω/□). Higher pyrolysis temperatures have previously been shown to reduce pyrolyzed polymer sheet resistance [10,13,23,24], but may also result in decreased porosity [16], as is briefly discussed below.

The theoretical energy density of the supercapacitor can be calculated using Eq. (2):

$$E = \frac{1}{2}CV^2 \quad (2)$$

where C is the capacitance, and V is the maximum voltage window. For a voltage window of −0.2 to 0.8 V, the theoretical energy density is calculated to be on the order of 1–1.5 mJ/cm^2 for the scan rates measured here, yielding volumetric energy densities of the order 10–15 mJ/cm^3.

A long-term stability test is performed via repetitive CV scans at a scan rate of 100 mV/s. The capacitance values, as obtained using Eq. (1) and normalized to the initial value, are presented in Fig. 5. Although the reason for the initial decline is not known, the results demonstrate the excellent long-term stability of the film in an aqueous electrolyte. A second stability test, performed at a scan rate of 5 V/s over 500,000 cycles shows similar behavior. This robust performance compares favorably to those reported by Beidaghi et al., that showed a 12% capacitance fade over only 1000 cycles for an electrochemically activated pyrolyzed SU-8 microsupercapacitor [14].

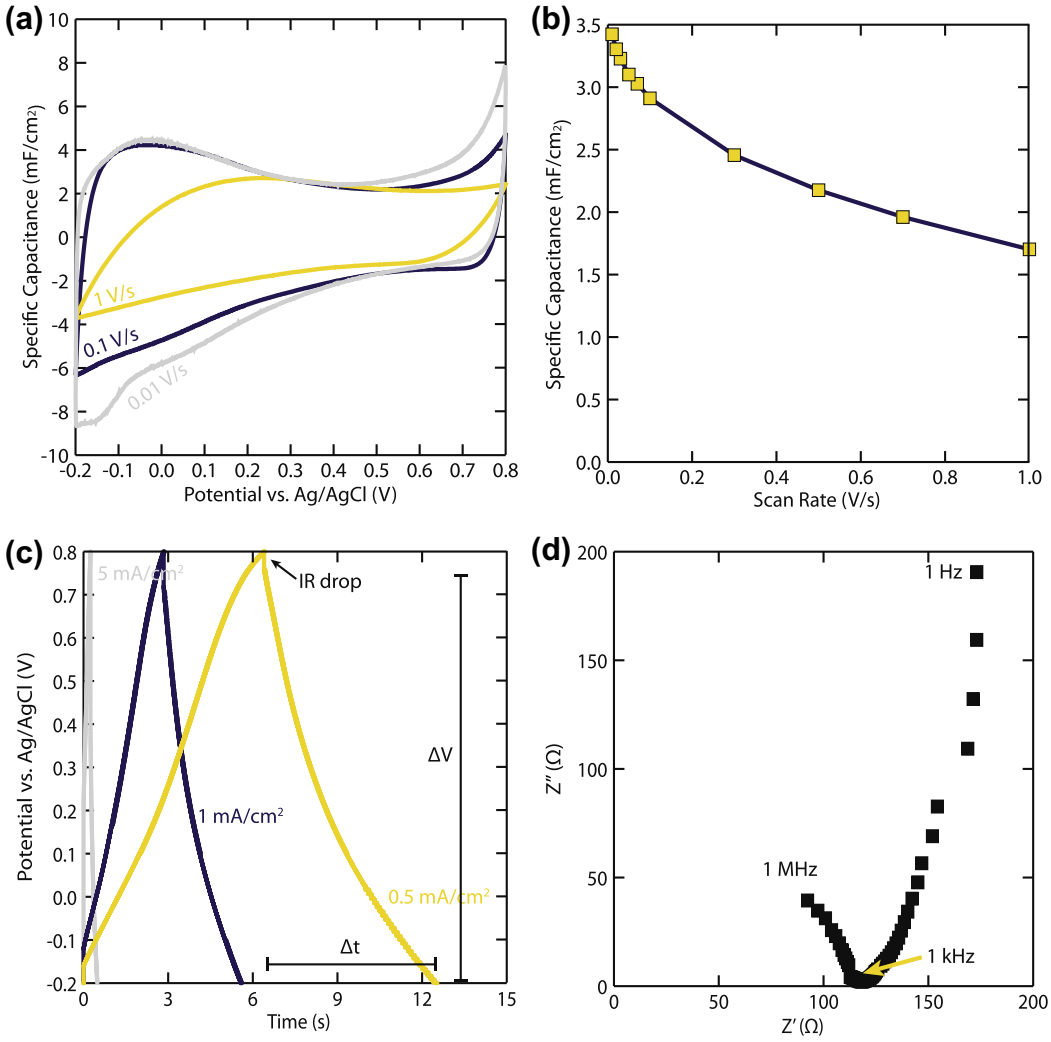

Fig. 4 – (a) Cyclic voltammograms for 1-μm thick pyrolyzed photoresist electrode. The specific current for each run is normalized by scan rate and plotted as "specific capacitance" for ease of viewing; the actual capacitance does not vary across the voltage sweep. (b) Specific capacitance, calculated from CV, at different scan rates. (c) Galvanostatic charge/discharge curves. The ΔV and Δt used for the capacitance calculation for the 0.5 mA/cm² scan are shown as an example. (d) AC impedance spectra. DC voltage is 0 V; AC amplitude is 5 mV. Electrolyte is 3.5 M KCl. Counter and reference electrodes are Pt and Ag/AgCl, respectively.

4. Discussion

The measured capacitance even at high scan rates of >1.5 mF/cm² is nearly three orders of magnitude higher than the values reported by Ranganathan et al. for AZ-4300 photoresist pyrolyzed at 1000 °C in 5% H_2/95% N_2 gas [13]. In order to probe the large disparity between these results, SPR-220-7 is pyrolyzed using the aforementioned parameters, but instead of using one gaseous environment for heating and another for pyrolysis as done in this paper, the 10% H_2/90% Ar gas is flowed throughout the entire procedure, including heating and cooling. This procedure is intended to emulate the previous works that employed forming gas throughout the procedure. These films yield specific capacitances on the order of 25 μF/cm², much lower than the values achieved here using the alternative two-gas procedure. Pyrolysis in an Ar-only environment is also probed, yielding a capacitance of ~200 μF/cm², also quite low relative to those annealed with the two-gas procedure. Starting with the same SPR-220 film thickness of 10 μm, the thickness after pyrolysis is measured via cross-sectional SEM to be 1.0, 0.95, and 1.1 μm for the films pyrolyzed in the two-gas, H_2/Ar only, and Ar only environments, respectively. For comparison, a SU-8-2007 film is also pyrolyzed using the two-gas procedure after subjecting it to a blanket exposure and development step, and the resulting capacitance is on the order of 1 mF/cm², similar to the SPR-220-7 film which has been the focus of the present paper. This result implies that within the range of parameters examined, it is the synthesis details, and not the choice of photoresist, that is responsible for the improved capacitance. Another procedural difference between this work and Refs. [13,14] is the final pyrolysis temperature (900 vs. 1000 °C). A test of

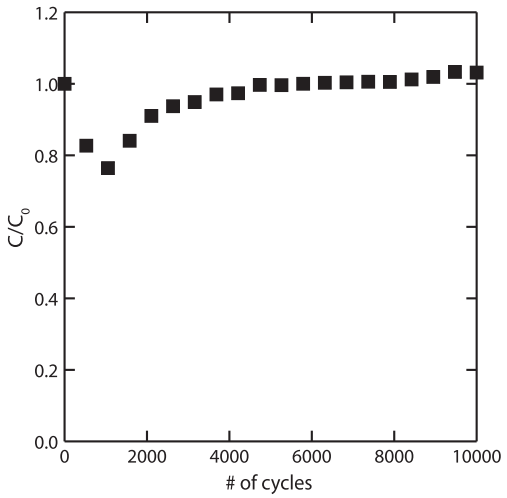

Fig. 5 – Plot of capacitance over 10,000 charge/discharge cycles, normalized by original capacitance value. Scan rate is 100 mV/s, and voltage window −0.2 to 0.8 V. Electrolyte is 3.5 M KCl. Counter and reference electrodes are Pt and Ag/AgCl, respectively.

the resultant film from the two-gas procedure at 1000 °C yielded significantly lower capacitance (<1 μF/cm^2) than that of the 900 °C film, likely due to decreased specific surface area in the film pyrolyzed at 1000 °C. The porosity of the pyrolyzed photoresist films is a result of the evolution of volatiles during pyrolysis [25]. Jenkins and Kawamura show that porosity of pyrolyzed phenolic resins (which are chemically similar to positive photoresists like SPR-220) depends highly on pyrolysis temperature, with a maximum micropore volume achieved at about 700 °C [16]. However, pyrolysis of photoresist at 700 °C yields a high resistance film [13,16]; a temperature of 900 °C is selected to optimize both parameters. The analysis indicates that the pyrolysis temperature, in addition to the two-gas procedure, is crucial for the formation of a porous film.

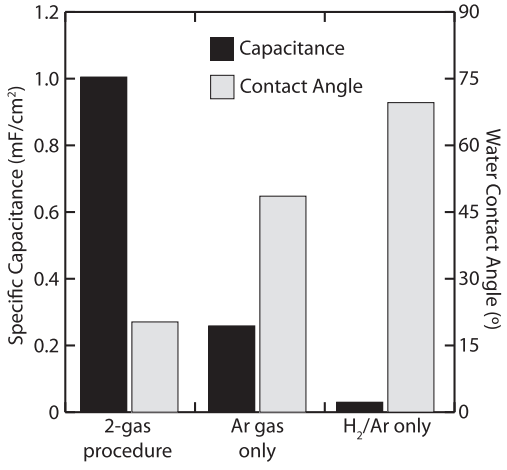

Fig. 6 – Comparison of SPR-220 films pyrolyzed under various gaseous environments. Capacitance is calculated from CV at a 100 mV/s scan rate. Water contact angle is shown on the right hand axis.

In order to probe the source of differences between the two-gas and one-gas pyrolyzed SPR-220 samples, water contact angle measurements are carried out (Fig. 6). Measurements show that the samples annealed with Ar/H_2 gas or Ar throughout are significantly more hydrophobic than those which result from the two-gas procedure. These results suggest improved electrolyte wetting of interior pore surfaces is likely responsible for the higher capacitance from the two-gas pyrolysis. The more hydrophilic the film, the greater the double layer surface area available for charging. As to the underlying mechanism for the variation in film wettability, Lyons et al. demonstrated that pyrolyzed phenolic resins differ in volumetric shrinkage depending on pyrolysis atmosphere: films pyrolyzed in pure N_2 are about twice as thick as those pyrolyzed in pure H_2, implying significant reactivity between the H_2 and the carbonizing film leading to a smaller, and perhaps denser film [24,26]. In our case, the thickness differences are not as large (1.1 vs. 0.95 μm for Ar vs. H_2/Ar), but follow the same general trend. Thermogravimetric analysis and mass spectrometry undertaken during pyrolysis in high vacuum or inert environments show that much of the mass loss occurs at $T < 600$ °C, and further carbonization occurs at higher temperatures but accounts for a small fraction of the overall mass loss [13,17,18,16]. Therefore, in our procedure, the majority of the carbonization likely proceeds primarily in an inert (Ar) environment and before H_2 is introduced. According to Lyons et al., this environment should lead to a thicker film than one in which H_2 is present throughout [24]. Introduction of H_2 at 900 °C can then lead to additional carbon removal, potentially by the etching of the pores. This high porosity can contribute to the low observed water contact angle (and improved wetting) of the two-gas pyrolyzed sample by capillary action. Unfortunately, the porosity of the films could not be reliably determined via BET analysis because the amount of material produced is too small to yield reliable adsorption measurements. This is an area that requires further investigation. The slightly improved wetting of the Ar-only sample compared to the forming gas only sample may be a result of more oxygen-containing functional groups on the Ar-only sample (confirmed via XPS, which showed a O:C ratio of 23% for the Ar-only procedure vs. 13% for both the two-gas and forming-gas only procedures) [27].

5. Conclusion

In summary, we have developed a highly porous carbon material from photoresist which is easily deposited and patterned and can be integrated into planar, on-chip supercapacitor applications. The capacitances achieved are on the same order of magnitude as other, more complex planar supercapacitor fabrication techniques and show robust cycle behavior exceeding half a million cycles. The process is readily scalable to large wafer fabrication and can be easily integrated into microdevice fabrication. Furthermore, the storage capacity can be tailored by modulating thickness via spin speed changes or additional spin coats. This fabrication method holds promise for the low-cost, facile production of on-chip supercapacitors for micro-energy storage.

Acknowledgments

We gratefully acknowledge the National Science Foundation Grants CMMI-0825531 and EEC-0832819 (through the Center of Integrated Nanomechanical Systems) and a Graduate Research Fellowship (BH), and DARPA S&T Center CIEMS.

REFERENCES

[1] Simon P, Gogotsi Y. Materials for electrochemical capacitors. Nat Mater 2008;7:845–54.
[2] Pandolfo AG, Hollenkamp AF. Carbon properties and their role in supercapacitors. J Power Sources 2006;157:11–27.
[3] Frackowiak E. Carbon materials for supercapacitor application. Phys Chem Chem Phys 2007;9:1774–85.
[4] Jiang YQ, Zhou Q, Lin L. Planar MEMS supercapacitor using carbon nanotube forests. Proc IEEE Micr Elect 2009:587–90.
[5] Pech D, Brunet M, Taberna PL, Simon P, Fabre N, Mesnilgrente F, et al. Elaboration of a microstructured inkjet-printed carbon electrochemical capacitor. J Power Sources 2010;195(4):1266–9.
[6] Liu CC, Tsai DS, Susanti D, Yeh WC, Huang YS, Liu FJ. Planar ultracapacitors of miniature interdigital electrode loaded with hydrous RuO_2 and RuO_2 nanorods. Electrochim Acta 2010;55(20):5768–74.
[7] Liu F, Gutes A, Laboriante I, Carraro C, Maboudian R. Graphitization of n-type polycrystalline silicon carbide for on-chip supercapacitor application. Appl Phys Lett 2011;99(11):112104.
[8] El-Kady MF, Strong V, Dubin S, Kaner RB. Laser scribing of high-performance and flexible graphene-based electrochemical capacitors. Science 2012;335:1326–30.
[9] Chmiola J, Largeot C, Taberna PL, Simon P, Gogotsi Y. Monolithic carbide-derived carbon films for micro-supercapacitors. Science 2010;328(5977):480–3.
[10] Kim J, Song X, Kinoshita K, Madou M, White R. Electrochemical studies of carbon films from pyrolyzed photoresist. J Electrochem Soc 1998;145(7):2314–9.
[11] Wang C, Taherabadi L, Jia G, Madou M, Yeh Y, Dunn B. C-MEMS for the manufacture of 3D microbatteries. Electrochem Solid-State Lett 2004;7:A435–8.
[12] Scheuller OJA, Brittain ST, Whitesides GM. Fabrication of glassy carbon microstructures by soft lithography. Sensor Actuator 1999;A72:125–39.
[13] Ranganathan S, McCreery R, Majji SM, Madou M. Photoresist-derived carbon for microelectromechanical systems and electrochemical applications. J Electrochem Soc 2000;147(1):277–82.
[14] Beidaghi M, Chen W, Wang C. Electrochemically activated carbon micro-electrode arrays for electrochemical micro-supercapacitors. J Power Sources 2011;196:2403–9.
[15] Beidaghi M, Wang C. Micro-supercapacitors based on three dimensional interdigital polypyrrole/C-MEMS electrodes. Electrochim Acta 2011;56:9508–14.
[16] Jenkins GM, Kawamura K. Polymeric carbons – carbon fibre, glass and char. London: Cambridge University Press; 1976.
[17] Lum R, Wilkins CW, Robbins M, Lyons AM, Jones RP. Thermal analysis of graphite and carbon-phenolic composites by pyrolysis–mass spectrometry. Carbon 1983;21:111–6.
[18] Xiang HQ, Fang SB, Jiang YY. Carbonaceous anodes for lithium-ion batteries prepared from phenolic resist with different cross-linking densities. J Electrochem Soc 1997;144:L187–90.
[19] Frackowiak E. Carbon materials for supercapacitor application. Phys Chem Chem Phys 2007;9:1774–85.
[20] Niu J, Pell WG, Conway BE. Requirements for performance characterization of C double-layer supercapacitors: applications to a high specific-area C-cloth material. J Power Sources 2006;156:725–40.
[21] Stoller MD, Ruoff RS. Best practice methods for determining an electrode material's performance for ultracapacitors. Energy Environ Sci 2010;3:1294–301.
[22] Conway BE. Electrochemical supercapacitors: scientific fundamentals and technological applications. New York: Kluwer Academic/Plenum Publishers; 1999.
[23] Kinoshita K, Song X, Kim J, Inaba M. Development of a carbon-based lithium microbattery. J Power Sources 1999;81–82:170–5.
[24] Lyons AM, Wilkins CW, Robbin M. Thin pinhole-free carbon films. Thin Solid Films 1983;103:333–41.
[25] Manocha SM. Porous carbons. Sadhana 2003;28:335–48.
[26] Lyons AM, Hale LP, Wilkins CW. Photodefinable carbon films: control of image quality. J Vac Sci Technol B 1985;3:447–52.
[27] Kuo TC, McCreery RL. Surface chemistry and electron-transfer kinetics of hydrogen-modified glassy carbon electrodes. Anal Chem 1999;71:1553–60.